Plasmonic-type acoustic cloak made of a bilaminate shell

Matthew D. Guild,[1,2,*] Michael R. Haberman,[1,2] and Andrea Alù[3]
[1]*Applied Research Laboratories, The University of Texas at Austin, Austin, Texas 78713-8029, USA*
[2]*Department of Mechanical Engineering, The University of Texas at Austin, Austin, Texas 78712-1024, USA*
[3]*Department of Electrical and Computer Engineering, The University of Texas at Austin, Austin, Texas 78712-0240, USA*
(Received 16 June 2012; published 7 September 2012)

Alternating isotropic layers have been widely used in the design of acoustic cloaks to achieve the necessary anisotropy required by coordinate-transformation techniques. In this paper, this concept is expanded to plasmonic-type acoustic cloaking using a bilaminate shell consisting of two isotropic layers with uniform thickness. Explicit analytic expressions based on thin-shell approximations for the necessary cloaking layer properties are developed, facilitating an examination of the fundamental physical behavior and dominant design parameters for a bilaminate plasmonic-type acoustic cloak. Based on this analysis, the performance of a bilaminate plasmonic-type acoustic cloak is examined, and practical means of achieving the desired cloaking layer properties are discussed.

DOI: 10.1103/PhysRevB.86.104302 PACS number(s): 43.40.Fz, 43.40.Sk, 43.20.Fn

I. INTRODUCTION

An exciting technique to achieve cloaking can be accomplished using a *plasmonic cloak*, which is a nonresonant means of canceling the scattered field from an object, thereby hiding it from detection. This was originally applied and demonstrated for electromagnetic waves,[1,2] using plasmonic materials to achieve the necessary cloaking layer properties, and has recently been shown to also be an effective means of cloaking acoustic waves.[3,4] Unlike cloaks developed using a coordinate-transformation approach,[5,6] only the scattered field in the surrounding medium is eliminated, and therefore this solution does not limit the incident wave from interacting with the object. As a result, there is no restriction on the use of isotropic materials to create a plasmonic cloak, and the cloak may be used to suppress the scattering from sensors and receiving devices.[7,8]

In realistic implementations, transformation-based cloaks invariably allow a small amount of energy enter the object. Recent work has examined amplification of these waves inside an acoustic cloak to realize invisible sensors based on transformation cloaks.[9,10] Realization for this has been proposed using an acoustic *anticloak,*[10] although this requires the use of anisotropic *double-negative* acoustic metamaterials, which are difficult to achieve and are inherently narrow band. Also, *superlensing* has been investigated as an effective means of cloaking an acoustic sensor.[11,12] Cloaks of this type, unlike plasmonic cloaks, utilize amplification of the evanescent waves, or *anomalous resonances*, which require the use of *single-negative* material properties.[13]

Previous work has shown that the use of a single fluid or isotropic elastic solid could be used to significantly reduce the scattering strength of acoustic waves from a submerged sphere at low frequencies, analogous to plasmonic cloaking for acoustic waves.[3,4] Compared to the electromagnetic case, the cancellation of scattered acoustic waves using a single isotropic layer provided much larger bandwidth. This arises from the inherent frequency dispersion of plasmonic materials for electromagnetic waves and the associated limitations due to causality, which reduce the effective bandwidth.[4,14] Even if plasmonic effects are not available for acoustic waves, the same plasmoniclike properties can be achieved using ordinary fluids or isotropic elastic solids, with material properties either much smaller or much larger than those of the the surrounding medium as needed. Furthermore, causality restrictions are relaxed since in this scenario the acoustic wave generally travels at velocities much smaller than that of light in free space.

One of the limitations of the single-layer cloaks analyzed previously was the small size of the objects to be cloaked compared to the wavelength of excitation.[3,4] To create a robust plasmonic-type acoustic cloak for larger objects, a multilayered structure must be considered. Furthermore, different core materials require different cloaking layer properties, so a multilayer design allows for more degrees of freedom. The focus of this work is on a bilaminate shell made up of two isotropic layers of uniform thickness. Although relatively simple in design, this structure enables a much wider range of dynamic behavior than a single layer, including anisotropic inertial effects.[15] In fact, the use of alternating fluid layers has been widely proposed as a practical method for realizing transformation-based acoustic cloaks.[16,17]

To facilitate the design of a bilaminate plasmonic-type acoustic cloak for an arbitrary spherical scatterer, analytic expressions are developed for two thin fluid shells. The functional dependence of the cloaking layer properties on the input design parameters are examined. Based on the results of this analysis, the design of a bilaminate plasmonic-type acoustic cloak for a steel sphere in water is illustrated. Finally, practical considerations are addressed, including feasibility of achieving the required material properties and the effects of elasticity on the cloak performance.

II. BACKGROUND

In order to investigate the nature of plasmonic-type acoustic cloaking, consider the classical formulation for the scattering of a time-harmonic plane wave impinging upon an isotropic elastic sphere coated by two fluid layers of uniform thickness as illustrated in Fig. 1. The solution for the scattered pressure in the surrounding fluid can be written as a summation of spherical harmonics

$$p_{\mathrm{sc}} = p_0 e^{-i\omega t} \sum_{n=0}^{\infty} i^n (2n+1)\, A_n h_n^{(1)}(k_{\mathrm{d},0} r) P_n(\cos\theta), \quad (1)$$

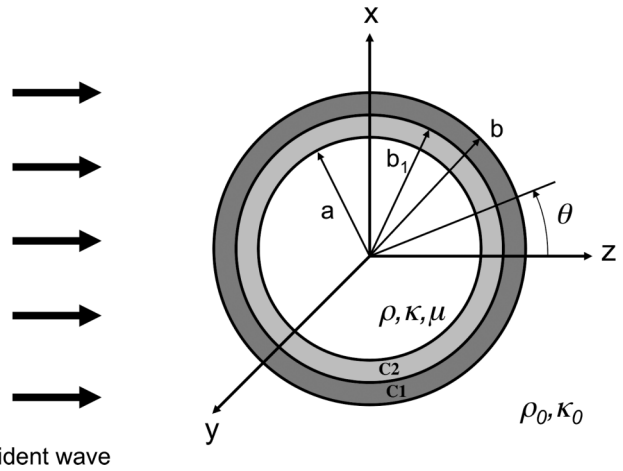

FIG. 1. A time-harmonic incident plane wave in a fluid medium impinging on an isotropic elastic core of radius a coated in two concentric shells of uniform thickness with outer radius b. The surrounding medium has density ρ_0 and bulk modulus κ_0, and the elastic core has density ρ, bulk modulus κ, and shear modulus μ.

where p_0 is the amplitude of the incident wave, $h_n^{(1)}$ is the spherical Hankel function of the first kind, $k_{\mathrm{d},0}$ is the wave number in the surrounding fluid, P_n is the Legrendre polynomial, and θ is the polar angle. A_n is the scattering coefficient for the nth mode, and is determined by the specific configuration of the coated sphere, including the material properties, the number of layers, and the thickness of each.

In a similar manner, the stress and displacement field within the elastic sphere and shells can be found through an expansion using spherical harmonics, the coefficients of which are the scattering coefficients for the wave field in each layer. Use of the same form as Eq. (1) for the fields present in each layer leads to

$$p_{\mathrm{c}1} = p_0 e^{-i\omega t} \sum_{n=0}^{\infty} i^n (2n+1) P_n(\cos\theta) \times [B_n j_n(k_{\mathrm{d},\mathrm{c}1} r) + C_n n_n(k_{\mathrm{d},\mathrm{c}1} r)], \tag{2}$$

$$p_{\mathrm{c}2} = p_0 e^{-i\omega t} \sum_{n=0}^{\infty} i^n (2n+1) P_n(\cos\theta) \times [D_n j_n(k_{\mathrm{d},\mathrm{c}2} r) + E_n n_n(k_{\mathrm{d},\mathrm{c}2} r)], \tag{3}$$

where B_n and C_n are the scattering coefficients in the outer cloaking layer, D_n and E_n are the scattering coefficients in the inner cloaking layer, and j_n and n_n are the spherical Bessel functions of the first and second kinds, respectively.

A linear system of equations for the nth mode are obtained by applying the boundary conditions at the interfaces of each surface,

$$\boldsymbol{\mathcal{D}}^{(n)} \cdot \vec{\mathcal{A}}^{(n)} = \vec{\mathrm{r}}^{(n)}, \tag{4}$$

where $\boldsymbol{\mathcal{D}}^{(n)}$ is the system matrix with coefficients containing the material properties and shell geometry, $\vec{\mathrm{r}}^{(n)}$ is the input vector describing the incident wave, and $\vec{\mathcal{A}}^{(n)}$ is a vector containing the unknown scattering coefficients in the central sphere, in each layer, and in the surrounding medium. To determine the scattered field in the surrounding fluid, Cramer's rule can be used to solve Eq. (4) for the scattering coefficient of the nth in the surrounding fluid,

$$A_n = \frac{\det \boldsymbol{\mathcal{R}}^{(n)}}{\det \boldsymbol{\mathcal{D}}^{(n)}}, \tag{5}$$

where $\boldsymbol{\mathcal{D}}^{(n)}$ is the system matrix and $\boldsymbol{\mathcal{R}}^{(n)}$ is $\boldsymbol{\mathcal{D}}^{(n)}$ with the first column replaced by $\vec{\mathrm{r}}^{(n)}$.

This implementation is a well-established approach which has been used to calculate acoustic scattering from an elastically coated elastic sphere and can be found in scientific literature on the subject dating back to the 1950s,[18–22] including detailed work accounting for viscous and thermal effects.[23] In all these previous works, the scattering coefficients and the resulting scattered field have been determined for specific shell and core properties. For such cases, the coefficients of $\boldsymbol{\mathcal{R}}^{(n)}$ and $\boldsymbol{\mathcal{D}}^{(n)}$ are specified and the unknown scattering coefficient in the surrounding fluid can be solved explicitly using Eq. (5).

When the material properties and geometry are known, the scattering coefficients for each mode can be calculated using Eq. (5), and determination of the scattered field is straightforward. To quantify the scattering strength of an object, the *total scattering cross section* can be expressed as

$$\sigma_{\mathrm{total}}(r) = \frac{4\pi}{|k_{\mathrm{d},0}|^2} \sum_{n=0}^{\infty} (2n+1)|A_n|^2, \tag{6}$$

which represents a measure of the acoustic power scattered relative to the incident wave over all angles.

For the case of acoustic cloaking, a solution is sought where the incident compressional wave passes unimpeded around the target. Mathematically, this means that the total acoustic field is equal to the incident wave throughout the surrounding fluid, which requires that the scattered field throughout the surrounding fluid approaches zero. Written in terms of the scattering coefficient, this corresponds to the condition where $A_n = 0$ for each relevant mode n of the expansion. Thus, under this condition, the total scattering cross section can be made very small and the scattered acoustic energy may be suppressed, thereby achieving *scattering cancellation*.

Letting $\boldsymbol{\mathcal{R}}^{(n)} = -\mathbf{U}^{(n)}$ and $\boldsymbol{\mathcal{D}}^{(n)} = \mathbf{U}^{(n)} + i\mathbf{V}^{(n)}$, Eq. (5) can be expressed as[4]

$$A_n = \frac{-\mathrm{U}^{(n)}}{\mathrm{U}^{(n)} + i\mathrm{V}^{(n)}}, \tag{7}$$

where $\mathrm{U}^{(n)} = \det \mathbf{U}^{(n)}$ and $\mathrm{V}^{(n)} = \det \mathbf{V}^{(n)}$. This expression indicates that the scattering cancellation of a given mode is achieved by finding cloak properties that lead to $\mathrm{U}^{(n)} = 0$, provided that $\mathrm{V}^{(n)} \neq 0$. Conversely, when $\mathrm{V}^{(n)} = 0$, A_n has a magnitude of unity for any nonzero value of $\mathrm{U}^{(n)}$ corresponding to a modal scattering resonance.

To obtain the cloaking layer properties, $\mathrm{U}^{(n)} = 0$ must be solved for each scattering mode. Given a finite number of layers, only a finite number of the leading-order modes can simultaneously be canceled. To obtain these properties, the system of equations must be solved implicitly. Although there are various ways to solve such a system, the method implemented here utilizes a quasi-Newton minimization algorithm employing sequential quadratic programming (SQP).[3,4] We apply this numerical technique to optimize the cloaking layer properties in the multidimensional parameter space and determine the optimal design parameters that satisfy this

condition at the frequency of interest. To determine the solution for $\mathrm{U}^{(n)} = 0$ using such an algorithm, the user specifies the design frequency and shell thicknesses, and provides an initial guess of the material properties of the cloak. To perform this operation, a code was implemented in MATLAB using the *fminsearch* function.[24]

Although the implementation of a numerical solver is relatively straightforward, it is important to note that the output of such an algorithm is a function of the initial guess given to the system. For the case of a single cloaking layer, previous work by the authors has shown that an estimate for the initial guess can be obtained either using parametric studies of the cloaking layer properties and relevant geometric properties,[3] or quasistatic expressions for the cloaking layer density and bulk modulus.[4]

In addition to determining estimates for the initial guesses, parametric studies for the case of a single cloaking layer have revealed the existence of two distinct types of modal cancellation, the nonresonant *plasmonic* type of interest in this work, and those arising from modal *antiresonances*.[4] Although both satisfy the condition $A_n = 0$, antiresonance modes occur beyond the first resonance of the cloaking layer, leading to a significantly different internal field distribution and smaller bandwidths.

An important question when solving for the cloaking layer properties of a bilaminate shell, therefore, is whether or not the minimized solution represents a local minimum or a global minimum, and if it represents *plasmonic* or *antiresonance* scattering cancellation. To ensure that optimal solutions are found, it is crucial to understand the nature of the design space, and what type of cloaking layers are necessary to achieve scattering cancellation.

Through the use of only a single fluid layer, significant reductions in the total scattering cross section of up to 40 dB were achieved at the design frequency. However, with two design parameters, the density and bulk modulus of the fluid cloaking layer, only the first two scattering modes could be simultaneously canceled, limiting the functionality of the cloak to rather small objects. The most practical means to achieve the cancellation of multiple modes is to consider a design consisting of multiple layers, which offers more degrees of freedom. Even for the relatively simple case of two fluid cloaking layers, however, this results in three additional parameters (density, bulk modulus, and shell thickness), making the already complex parameter space impractical to analyze using parametric studies only. To investigate the necessary layer properties for our initial guess, therefore, a thin-shell analytic solution is developed for a plasmonic-type bilaminate shell consisting of two fluid layers at moderate frequencies, as discussed in the next section.

III. ANALYTIC FORMULATION OF THE CLOAKING LAYER PROPERTIES

The simplest case of a multilayered plasmonic-type acoustic cloak will be considered here, consisting of two thin fluid shells. Although at first glance this may only appear to represent a modest increase in complexity over the single-layer solutions developed previously,[4] there are several important novel features of the two-layer plasmonic cloak. First, the properties of each of the two fluid layers may be significantly different from each other, and from those of a single layer. Understanding these differences is important for the development of more complicated multilayered acoustic plasmonic-type cloaks. Second, due to the increased complexity of the expressions and the presence of additional cloaking layer parameters, the analytic formulation developed for two fluid layers does not reduce to compact, explicit expressions, as was achieved for a single layer. Instead, a system of coupled equations is developed that can be solved implicitly, and can be generalized to multilayered configurations. Finally, and probably most importantly, the two-layer acoustic plasmonic-type cloak demonstrates one of the key benefits of using a plasmonic cloak consisting of multiple isotropic layers, that the addition of more layers allows for the simultaneous cancellation of more modes.

For the case of an isotropic elastic core coated with two fluid layers, consistent with Fig. 1, Eq. (7) becomes

$$\begin{vmatrix} u_{11}^{(n)} & u_{12}^{(n)} & u_{13}^{(n)} & 0 & 0 & 0 & 0 \\ u_{21}^{(n)} & u_{22}^{(n)} & u_{23}^{(n)} & 0 & 0 & 0 & 0 \\ 0 & u_{32}^{(n)} & u_{33}^{(n)} & u_{34}^{(n)} & u_{35}^{(n)} & 0 & 0 \\ 0 & u_{42}^{(n)} & u_{43}^{(n)} & u_{44}^{(n)} & u_{45}^{(n)} & 0 & 0 \\ 0 & 0 & 0 & u_{54}^{(n)} & u_{55}^{(n)} & u_{56}^{(n)} & u_{57}^{(n)} \\ 0 & 0 & 0 & u_{64}^{(n)} & u_{65}^{(n)} & u_{66}^{(n)} & u_{67}^{(n)} \\ 0 & 0 & 0 & 0 & 0 & u_{76}^{(n)} & u_{77}^{(n)} \end{vmatrix} = 0, \tag{8}$$

where the nonzero terms are given in Appendix A.

Examining Eqs. (8) and (A1)–(A24), one notes that the elements in different columns in Eq. (8) are functions of only a single material property: column 1 depends on the surrounding fluid properties, columns 2 and 3 on the outer cloaking layer, columns 4 and 5 on the inner cloaking layer, and columns 6 and 7 on the elastic core material. Evaluation of the determinant given by Eq. (8) yields

$$\begin{aligned} &\left[\eta_{11}^{(n)} - \eta_{12}^{(n)}\right]\left[u_{44}^{(n)}\left(u_{55}^{(n)} - \Upsilon_n u_{65}^{(n)}\right) - u_{45}^{(n)}\left(u_{54}^{(n)} - \Upsilon_n u_{64}^{(n)}\right)\right] \\ &\quad - \left[\eta_{21}^{(n)} - \eta_{22}^{(n)}\right]\left[u_{34}^{(n)}\left(u_{55}^{(n)} - \Upsilon_n u_{65}^{(n)}\right)\right. \\ &\quad \left. - u_{35}^{(n)}\left(u_{54}^{(n)} - \Upsilon_n u_{64}^{(n)}\right)\right] = 0, \end{aligned} \tag{9}$$

where

$$\eta_{11}^{(n)} = u_{11}^{(n)}\left[u_{22}^{(n)}u_{33}^{(n)} - u_{23}^{(n)}u_{32}^{(n)}\right], \tag{10}$$

$$\eta_{12}^{(n)} = u_{21}^{(n)}\left[u_{12}^{(n)}u_{33}^{(n)} - u_{13}^{(n)}u_{32}^{(n)}\right], \tag{11}$$

$$\eta_{21}^{(n)} = u_{11}^{(n)}\left[u_{22}^{(n)}u_{43}^{(n)} - u_{23}^{(n)}u_{42}^{(n)}\right], \tag{12}$$

$$\eta_{22}^{(n)} = u_{21}^{(n)}\left[u_{12}^{(n)}u_{43}^{(n)} - u_{13}^{(n)}u_{42}^{(n)}\right], \tag{13}$$

and

$$\Upsilon_n = \begin{cases} \frac{u_{56}^{(n)}u_{77}^{(n)} - u_{57}^{(n)}u_{76}^{(n)}}{u_{66}^{(n)}u_{77}^{(n)} - u_{67}^{(n)}u_{76}^{(n)}} & \text{for an elastic core,} \\ \frac{u_{56}^{(n)}}{u_{66}^{(n)}} & \text{for a fluid core.} \end{cases} \tag{14}$$

Examining Eqs. (10)–(13) shows that these terms are only dependent on the material properties of the outer fluid cloaking layer and the surrounding fluid medium. Likewise, the terms

$u_{i4}^{(n)}$ and $u_{i5}^{(n)}$ (with $i = 3$, 4, 5, or 6) appearing in Eq. (9) are only dependent on the material properties of the inner fluid cloaking layer. Through the definition of Υ_n given by Eq. (14), the core material properties can be written in terms of a single parameter. Therefore, it can be seen that the bracketed items in Eq. (9) contain terms which depend on either the inner cloaking layer properties (and the core material properties), or the outer cloaking layer properties (and the surrounding fluid properties).

Although Eq. (9) represents a relatively compact expression for the cloaking condition of the nth mode, its expansion by the substitution of the exact expressions in Eqs. (A1)–(A24) yields a complicated and virtually intractable equation. To reduce this expression to a manageable form while still retaining its practical applicability for finding layer properties leading to plasmonic-type acoustic cloaking, a thin-shell approximation can be made. For the components of the determinant $\mathrm{U}^{(n)}$ which describe the cloaking layers, expansion of the Taylor series about the interface between the two layers $r = b_1$ yields

$$j_n(k_{\mathrm{d,c1}}b) \approx j_n(k_{\mathrm{d,c1}}b_1) + (k_{\mathrm{d,c1}}b_1\delta_1)\, j_n'(k_{\mathrm{d,c1}}b_1) + (k_{\mathrm{d,c1}}b_1\delta_1)^2 j_n''(k_{\mathrm{d,c1}}b_1), \tag{15}$$

$$j_n(k_{\mathrm{d,c2}}a) \approx j_n(k_{\mathrm{d,c2}}b_1) - (k_{\mathrm{d,c2}}b_1\delta_2)\, j_n'(k_{\mathrm{d,c2}}b_1) + (k_{\mathrm{d,c2}}b_1\delta_2)^2 j_n''(k_{\mathrm{d,c2}}b_1), \tag{16}$$

where $\delta_1 = (b - b_1)/a$ and $\delta_2 = (b_1 - a)/a$ are the shell thicknesses of the outer and inner cloaking layers, respectively, normalized by the core radius a. Expressions similar to Eqs. (15) and (16) may be written for any other spherical Bessel function. In these equations, terms of order $(k_{\mathrm{d,c}}b_1\delta)^2$ have been retained to ensure sufficient accuracy in the resulting expressions for the cloaking layer properties. Even though it will be assumed that the shells are geometrically small ($\delta \ll 1$), large values of the outer layer density are required in some cases, so that the wave number within the layer does not satisfy the condition $k_{\mathrm{d,c}}a\,\delta \ll 1$. However, by retaining the second-order terms, the less restrictive condition of $(k_{\mathrm{d,c}}a\,\delta)^2 \ll 1$ can be applied.

To evaluate the cloaking condition using two fluid layers, a thin-shell approximation is obtained by substituting Eqs. (A1)–(A24) and (15) and (16) into Eqs. (9)–(14). After some algebraic manipulation and neglecting terms of order δ^3, and making use of the relationships between the products of spherical Bessel functions and their derivatives,

$$j_n(z)n_n'(z) - j_n'(z)n_n(z) = z^{-2}, \tag{17}$$

$$j_n(z)n_n''(z) - j_n''(z)n_n(z) = -2z^{-3}, \tag{18}$$

$$j_n'(z)n_n''(z) - j_n''(z)n_n'(z) = z^{-2}[1 - l_n z^{-2}], \tag{19}$$

$$j_n(z)n_n'''(z) - j_n'''(z)n_n(z) = -z^{-2}[1 - (l_n + 6)z^{-2}], \tag{20}$$

$$j_n'(z)n_n'''(z) - j_n'''(z)n_n'(z) = -2z^{-3}[1 - 2\,l_n z^{-2}] \tag{21}$$

yields

$$\overline{\gamma}_n + \Upsilon_n\overline{\mathcal{F}}_n'[\overline{\rho}_{\mathrm{c1}}\delta_1 + \overline{\rho}_{\mathrm{c2}}\delta_2] - l_n\left\{\overline{\mathcal{F}}_n\left[\frac{\delta_1}{\overline{\rho}_{\mathrm{c1}}} + \frac{\delta_2}{\overline{\rho}_{\mathrm{c2}}}\right] - \frac{\overline{\rho}_{\mathrm{c1}}}{\overline{\rho}_{\mathrm{c2}}}\delta_1\delta_2 k_{\mathrm{d},0}b_1\, j_n'(k_{\mathrm{d},0}b_1) + \frac{\overline{\rho}_{\mathrm{c2}}}{\overline{\rho}_{\mathrm{c1}}}\delta_1\delta_2\Upsilon_n j_n(k_{\mathrm{d},0}b_1)\right\}$$
$$+ (k_{\mathrm{d},0}b_1)^2\left\{[\overline{\mathcal{F}}_n - \overline{\rho}_{\mathrm{c1}}\delta_1\overline{\mathcal{G}}_n + \overline{\rho}_{\mathrm{c2}}\delta_2\Upsilon_n j_n(k_{\mathrm{d},0}b_1)]\frac{\delta_1}{\overline{\kappa}_{\mathrm{c1}}} + [\overline{\mathcal{F}}_n - \overline{\rho}_{\mathrm{c1}}\delta_1 k_{\mathrm{d},0}b_1 j_n'(k_{\mathrm{d},0}b_1) - \overline{\rho}_{\mathrm{c2}}\delta_2\overline{\mathcal{G}}_n]\frac{\delta_2}{\overline{\kappa}_{\mathrm{c2}}}\right\} = 0, \tag{22}$$

where $l_n = n(n + 1)$ and

$$\overline{\mathcal{F}}_n = j_n(k_{\mathrm{d},0}b_1) + k_{\mathrm{d},0}b_1\,\delta_1\, j_n'(k_{\mathrm{d},0}b_1), \tag{23}$$

$$\overline{\mathcal{F}}_n' = k_{\mathrm{d},0}b_1[(1 + \delta_1)\, j_n'(k_{\mathrm{d},0}b_1) + k_{\mathrm{d},0}a\,\delta_1\, j_n''(k_{\mathrm{d},0}b_1)], \tag{24}$$

$$\overline{\mathcal{G}}_n = k_{\mathrm{d},0}b_1\, j_n'(k_{\mathrm{d},0}b_1) - \Upsilon_n j_n(k_{\mathrm{d},0}b_1), \tag{25}$$

$$\overline{\gamma}_n = (1 + \delta_2)\overline{\mathcal{F}}_n' - \Upsilon_n\overline{\mathcal{F}}_n + k_{\mathrm{d},0}b_1\, j_n'(k_{\mathrm{d},0}b_1)\left[\delta_2^2[2\,l_n + 6] + \delta_1^2 l_n\right] + \Upsilon_n j_n(k_{\mathrm{d},0}b_1)\left[\delta_1 + \delta_2^2 l_n + \delta_1^2[2\,l_n + 6]\right]. \tag{26}$$

It is important to note that Equations (17)–(21) are not based on any approximations, but are exact expressions derived using the relationship between derivatives based on the recursion relations of spherical Bessel functions.[25] Through the use of these identities, the transcendental relation among the cloaking layer properties may be replaced by the much simpler algebraic relation (22).

Based on previous investigations of multilayered fluids[15] and the use of these structures for acoustic metamaterials and cloaking applications,[16,26] one would expect the benefits of increasing the number of fluid layers to be dominated by the inertial effects of each layer. To illustrate this, consider first the case in which the densities of each layer are the same, so that $\overline{\rho}_{\mathrm{c1}} = \overline{\rho}_{\mathrm{c2}} \equiv \overline{\rho}_{\mathrm{c0}}$. In this case, to leading order (neglecting δ^2 terms), Eq. (22) reduces to

$$\overline{\gamma}_n + \Upsilon_n\overline{\mathcal{F}}_n'\overline{\rho}_{\mathrm{c0}}\delta_0 + (k_{\mathrm{d},0}b_1)^2\overline{\mathcal{F}}_n\frac{\delta_0}{\overline{\kappa}_{\mathrm{c0}}} - l_n\overline{\mathcal{F}}_n\frac{\delta_0}{\overline{\rho}_{\mathrm{c0}}} = 0, \tag{27}$$

where $\delta_0 = \delta_1 + \delta_2$ and

$$\frac{1}{\overline{\kappa}_{\mathrm{c0}}} = \left[\frac{\delta_1}{\delta_0}\frac{1}{\overline{\kappa}_{\mathrm{c1}}} + \frac{\delta_1}{\delta_0}\frac{1}{\overline{\kappa}_{\mathrm{c2}}}\right]. \tag{28}$$

From this relationship, it is clear that the bulk moduli $\overline{\kappa}_{\mathrm{c1}}$ and $\overline{\kappa}_{\mathrm{c2}}$ independently have very little effect (appearing only in terms of order δ^2), being dominated instead by the harmonic mean $\overline{\kappa}_{\mathrm{c0}}$. Even though the bulk moduli of each layer can be independently varied, the effective bulk modulus dominates the scattering cancellation effect for the first two scattering modes. Therefore, having two fluid layers with the same density does not allow for additional scattering modes to be canceled compared to a single layer. For this reason, we focus on cases in which the densities in the two layers are very different: (1) $\overline{\rho}_{\mathrm{c1}} \gg \overline{\rho}_{\mathrm{c2}}$ and (2) $\overline{\rho}_{\mathrm{c1}} \ll \overline{\rho}_{\mathrm{c2}}$. Within each one of these limits, Eq. (22) reduces to a simpler form, allowing for explicit expressions to be obtained for the cloaking conditions of the bilaminate layer.

A. Region 1: $\overline{\rho}_{c1} \gg \overline{\rho}_{c2}$

For the special case in which $\overline{\rho}_{c1} \gg \overline{\rho}_{c2}$, Eq. (22) simplifies to

$$\overline{\gamma}_n + \Upsilon_n \overline{\mathcal{F}}_n' \overline{\rho}_{c1}\delta_1 + (k_{d,0}b_1)^2 \left\{ [\overline{\mathcal{F}}_n - \overline{\rho}_{c1}\delta_1 \overline{\mathcal{G}}_n] \frac{\delta_1}{\overline{\kappa}_{c1}} + [\overline{\mathcal{F}}_n - \overline{\rho}_{c1}\delta_1 k_{d,0}b_1 j_n'(k_{d,0}b_1) + \overline{\rho}_{c2}\delta_2 \Upsilon_n j_n(k_{d,0}b_1)] \frac{\delta_2}{\overline{\kappa}_{c2}} \right\} - l_n \left\{ \overline{\mathcal{F}}_n \frac{\delta_2}{\overline{\rho}_{c2}} - \frac{\overline{\rho}_{c1}}{\overline{\rho}_{c2}} \delta_1\delta_2 k_{d,0}b_1 j_n'(k_{d,0}b_1) \right\} = 0. \quad (29)$$

To determine expressions for the cloaking layer properties, a system of equations can be obtained by writing Eq. (29) for the modes $n = 0$ through $n = 3$, in a similar manner to the approach taken for the single fluid layer.[3,4] However, cancellation of all four modes would require at least one negative parameter. In order to make the realization of the cloak simpler, the analysis is restricted instead to the range where $\overline{\rho}_{c1}$, $\overline{\kappa}_{c1}$, $\overline{\rho}_{c2}$, and $\overline{\kappa}_{c2}$ are all positive. Under this condition, a cloak will be sought which cancels the first three modes: $n = 0$ (monopole), $n = 1$ (dipole), and $n = 2$ (quadrupole).

With three equations prescribing the cancellation of each mode, only three of the cloaking layer properties will be explicitly determined, with the remaining property acting as a parameter. Thus, unlike the case of a single-fluid cloaking layer which has just one optimal solution, in this case a family of solutions is obtained. For the case of $\overline{\rho}_{c1} \gg \overline{\rho}_{c2}$, the three independent variables will be $\overline{\rho}_{c1}$, $\overline{\kappa}_{c1}$, and $\overline{\rho}_{c2}$, with $\overline{\kappa}_{c2}$ kept as a free parameter. To obtain solutions for each of the independent variables, each modal equation will be used to solve for one of the variables in terms of the others, systematically eliminating each of the variables. With $n = 0$, Eq. (29) reduces to

$$\overline{\kappa}_{c1} = \frac{\delta_1 (k_{d,0}b_1)^2 [\overline{\rho}_{c1}\delta_1 \overline{\mathcal{G}}_0 - \overline{\mathcal{F}}_0]}{\overline{\gamma}_0 + \overline{\rho}_{c1}\delta_1 \Upsilon_0 \overline{\mathcal{F}}_0' + (k_{d,0}b_1)^2 [\overline{\mathcal{F}}_0 - \overline{\rho}_{c1}\delta_1 k_{d,0}b_1 j_0'(k_{d,0}b_1) + \overline{\rho}_{c2}\delta_2 \Upsilon_0 j_0(k_{d,0}b_1)] \frac{\delta_2}{\overline{\kappa}_{c2}}}. \quad (30)$$

Substitution of Eq. (30) into (29) yields an expression relating the two remaining independent variables $\overline{\rho}_{c1}$ and $\overline{\rho}_{c2}$ and the parameter $\overline{\kappa}_{c2}$:

$$\left[\delta_2 \zeta_3^{(n)} \overline{\chi}_{c2}\right] \overline{\rho}_{c2}^2 + \left[\zeta_2^{(n)} + \zeta_1^{(n)} \overline{\chi}_{c2}\right] \overline{\rho}_{c2} - l_n \delta_2 \zeta_0^{(n)} = 0, \quad (31)$$

where $\overline{\chi}_{c2} = (k_{d,0}b_1)^2 \delta_2 / \overline{\kappa}_{c2}$ and

$$\zeta_m^{(n)} = a_m^{(n)} (\overline{\rho}_{c1}\delta_1)^2 + b_m^{(n)} \overline{\rho}_{c1}\delta_1 + c_m^{(n)}, \quad (32)$$

with $m = 0,1,2,$and 3, and the coefficients $a_m^{(n)}$, $b_m^{(n)}$, and $c_m^{(n)}$ given by Eqs. (B1)–(B12).

Through the use of Eq. (31) with $n = 1$, an expression for $\overline{\rho}_{c2}$ can be obtained which yields two roots, given by

$$\overline{\rho}_{c2}^{(1)} = \frac{2\delta_2 \zeta_0^{(1)}}{\zeta_2^{(1)} + \zeta_1^{(1)} (k_{d,0}b_1)^2 \frac{\delta_2}{\overline{\kappa}_{c2}}}, \quad (33)$$

$$\overline{\rho}_{c2}^{(2)} = -\frac{\zeta_2^{(1)} + \zeta_1^{(1)} (k_{d,0}b_1)^2 \frac{\delta_2}{\overline{\kappa}_{c2}}}{\delta_2 \zeta_3^{(1)} (k_{d,0}b_1)^2 \frac{\delta_2}{\overline{\kappa}_{c2}}}, \quad (34)$$

where the superscripts (1) and (2) denote the different roots of Eq. (31). From Eqs. (33) and (34), it is noted that $\overline{\rho}_{c2}^{(1)}$ is proportional to δ_2 and $\overline{\rho}_{c2}^{(2)}$ is proportional to δ_2^{-1}. Since $\delta_2 \ll 1$, this indicates that the magnitude of $\overline{\rho}_{c2}^{(1)}$ will be significantly smaller than $\overline{\rho}_{c2}^{(2)}$. Furthermore, comparing these roots to Eq. (31), it is observed that Eqs. (33) and (34) correspond to the solution for the limiting cases when $\overline{\rho}_{c2} \ll 1$ and $\overline{\rho}_{c2} \gg 1$, respectively. Therefore, to ensure validity of the assumption that $\overline{\rho}_{c1} \gg \overline{\rho}_{c2}$, the only valid root is the one given by Eq. (33). Although it is not apparent from Eq. (31), it will be seen later in this section that this root is positive within the range considered here.

To determine $\overline{\rho}_{c1}$, Eq. (33) is substituted into Eq. (31) with $n = 2$. A solution is sought such that $(\overline{\rho}_{c1}\delta_1)^2 \ll 1$ to ensure that $(k_{d,c1}b_1)^2 \ll 1$, which gives

$$q_2 (\overline{\rho}_{c1}\delta_1)^2 + q_1 \overline{\rho}_{c1}\delta_1 + q_0 = 0, \quad (35)$$

where the coefficients q_0, q_1, and q_2 are defined by Eqs. (B13)–(B15). From Eq. (35), a solution for $\overline{\rho}_{c1}$ can be obtained:

$$\overline{\rho}_{c1} = \frac{-q_1 \pm \sqrt{q_1^2 - 4q_0q_2}}{2\delta_1 q_2}. \quad (36)$$

Although this approximation is limited to relatively small values of $(\overline{\rho}_{c1}\delta_1)^2$, this solution can still result in a cloaking layer, the density of which is much larger than the surrounding fluid, given the requirement that $\delta_1 \ll 1$.

The results developed in this section permit direct calculation of the cloaking layer properties of a two-layer cloak with $(\overline{\rho}_{c1}\delta_1)^2$. Given a design frequency $k_{d,0}a$, and shell thicknesses δ_1 and δ_2, the properties $\overline{\kappa}_{c1}$, $\overline{\rho}_{c2}$, and $\overline{\rho}_{c1}$ can be determined using Eqs. (30), (33), and (36), respectively. The fourth cloaking layer property $\overline{\kappa}_{c2}$ is a free parameter, which leads to an entire family of possible designs.

B. Region 2: $\overline{\rho}_{c1} \ll \overline{\rho}_{c2}$

For the case in which $\overline{\rho}_{c1} \ll \overline{\rho}_{c2}$, Eq. (22) simplifies to

$$\overline{\gamma}_n + \Upsilon_n \overline{\mathcal{F}}_n' \overline{\rho}_{c2}\delta_2 + (k_{d,0}b_1)^2 \left\{ [\overline{\mathcal{F}}_n - \overline{\rho}_{c2}\delta_2 \overline{\mathcal{G}}_n] \frac{\delta_2}{\overline{\kappa}_{c2}} + [\overline{\mathcal{F}}_n - \overline{\rho}_{c1}\delta_1 k_{d,0}b_1 j_n'(k_{d,0}b_1) + \overline{\rho}_{c2}\delta_2 \Upsilon_n j_n(k_{d,0}b_1)] \frac{\delta_1}{\overline{\kappa}_{c1}} \right\} - l_n \left\{ \overline{\mathcal{F}}_n \frac{\delta_1}{\overline{\rho}_{c1}} + \frac{\overline{\rho}_{c2}}{\overline{\rho}_{c1}} \delta_1\delta_2 \Upsilon_n j_n(k_{d,0}b_1) \right\} = 0. \quad (37)$$

Comparing this expression to Eq. (29), one can see that both have the same basic form. Specifically, Eq. (37) can be

obtained from Eq. (29) by swapping $\overline{\rho}_{c1} \leftrightarrow \overline{\rho}_{c2}$, $\overline{\kappa}_{c2} \leftrightarrow \overline{\kappa}_{c1}$, and $\delta_2 \leftrightarrow \delta_1$. However, after performing this substitution, the two equations are not identical. In particular, terms containing $-k_{d,0}b_1 j_n'(k_{d,0}b_1)$ and $\Upsilon_n j_n(k_{d,0}b_1)$ in Eq. (29) correspond to terms containing $\Upsilon_n j_n(k_{d,0}b_1)$ and $-k_{d,0}b_1 j_n'(k_{d,0}b_1)$, respectively. Therefore, swapping $\Upsilon_n j_n(k_{d,0}b_1) \leftrightarrow -k_{d,0}b_1 j_n'(k_{d,0}b_1)$ in Eq. (37), in addition to swapping the inner and outer cloaking layer properties, yields an expression identical to Eq. (29).

Given the identical forms of Eqs. (29) and (37), an expression for $\overline{\kappa}_{c2}$ for the case when $\overline{\rho}_{c1} \ll \overline{\rho}_{c2}$ can be written as

$$\overline{\kappa}_{c2} = \frac{\delta_2 (k_{d,0}b_1)^2 [\overline{\rho}_{c2}\delta_2 \overline{\mathcal{G}}_0 - \overline{\mathcal{F}}_0]}{\overline{\gamma}_0 + \overline{\rho}_{c2}\delta_2 \Upsilon_0 \overline{\mathcal{F}}_0' + (k_{d,0}b_1)^2 [\overline{\mathcal{F}}_0 - \overline{\rho}_{c1}\delta_1 k_{d,0}b_1 j_0'(k_{d,0}b_1) + \overline{\rho}_{c2}\delta_2 \Upsilon_0 j_0(k_{d,0}b_1)] \frac{\delta_1}{\overline{\kappa}_{c1}}}. \tag{38}$$

In this case, the only differences in the coefficients given in Eqs. (B1)–(B9) are

$$\bar{a}_0^{(n)} = \Upsilon_n j_n(k_{d,0}b_1)\overline{\mathcal{G}}_0, \tag{39}$$

$$\bar{b}_0^{(n)} = \overline{\mathcal{F}}_n \overline{\mathcal{G}}_0 - \Upsilon_n j_n(k_{d,0}b_1)\overline{\mathcal{F}}_0, \tag{40}$$

$$\bar{a}_1^{(n)} = -k_{d,0}b_1 [\Upsilon_0 j_0(k_{d,0}b_1) j_n'(k_{d,0}b_1) - \Upsilon_n j_n(k_{d,0}b_1) j_0'(k_{d,0}b_1)], \tag{41}$$

$$\bar{b}_1^{(n)} = k_{d,0}b_1 [j_n(k_{d,0}b_1) j_0'(k_{d,0}b_1) - j_n'(k_{d,0}b_1) j_0(k_{d,0}b_1)]. \tag{42}$$

Therefore, Eqs. (39)–(42) are used in place of Eqs. (B1), (B2), (B4), and (B5) when $\overline{\rho}_{c1} \ll \overline{\rho}_{c2}$. Through the use of these terms, the cloaking layer densities are determined by

$$\overline{\rho}_{c1} = \frac{2\delta_1 \overline{\zeta}_0^{(1)}}{\overline{\zeta}_2^{(1)} + \overline{\zeta}_1^{(1)} (k_{d,0}b_1)^2 \frac{\delta_1}{\overline{\kappa}_{c1}}}, \tag{43}$$

$$\overline{\rho}_{c2} = \frac{-\bar{q}_1 \pm \sqrt{\bar{q}_1^2 - 4\bar{q}_0\bar{q}_2}}{2\delta_2 \bar{q}_2}, \tag{44}$$

where the coefficients $\overline{\zeta}_m^{(n)}$ and $\bar{q}_m^{(n)}$ (for $m = 0, 1,$ and 2) are obtained from Eqs. (32) and (B13)–(B15), respectively, evaluated using Eqs. (39)–(42).

For the case $\overline{\rho}_{c1} \ll \overline{\rho}_{c2}$, the three independent variables are $\overline{\kappa}_{c2}$, $\overline{\rho}_{c1}$, and $\overline{\rho}_{c2}$, with $\overline{\kappa}_{c1}$ remaining a free parameter. Given a design frequency $k_{d,0}a$, and shell thicknesses δ_1 and δ_2, the cloaking layer properties $\overline{\kappa}_{c2}$, $\overline{\rho}_{c1}$, and $\overline{\rho}_{c2}$ can be determined using Eqs. (38), (43), and (44) for a given value of $\overline{\kappa}_{c1}$.

IV. NUMERICAL RESULTS

The analysis in the previous section provides explicit solutions for the cloaking layer properties within a thin-shell approximation. Although evaluation of these expressions can enable significant insight into understanding the behavior of a two-layer plasmonic-type acoustic cloak, the solutions do not provide a simple interpretation or physical insight into the cloaking behavior, and the dependence on each input parameter is not obvious. Specifically, the value of the cloaking layer properties depends on the design frequency, shell thicknesses, and properties of the core material in nontrivial ways. In order to provide more insight into these general solutions, an investigation of how these input parameters affect the required cloaking layer properties for the limiting case of a rigid, immovable sphere is considered in the following section.

A. Cloaking of a rigid sphere using two fluid layers

The analytic expressions for the cloaking layer properties developed above are best understood by investigating a limiting case that is representative of practical conditions of interest. The specific limiting case of a rigid, immovable core has been selected for this purpose. This limit is obtained with a two-step process, first by applying the condition $\kappa \to \infty$ for a *rigid* scatterer, followed by taking the limit $\rho \to \infty$ for an *immovable* scatterer.[19] Note that for an isotropic elastic core material, the shear modulus can be written in terms of the bulk modulus κ and Poisson's ratio ν as $\mu = \frac{3}{2}\kappa(1-2\nu)/(1+\nu)$. With the physical bounds on Poisson's ratio for an elastic solid limited to $-1 \leqslant \nu < \frac{1}{2}$, taking $\kappa \to \infty$ corresponds to $\mu \to \infty$.[27]

These limits must be taken for the function Υ_n in Eq. (14), which contains all the terms involving the properties of the core material. In the quasistatic limit, Υ_n for an isotropic elastic sphere becomes

$$\Upsilon_0 = -\frac{1}{3\overline{\kappa}}(k_{d,0}a)^2, \tag{45}$$

$$\Upsilon_1 = \frac{1}{\overline{\rho}}, \tag{46}$$

$$\Upsilon_2 = -\frac{1}{2\overline{\mu}} \frac{\left(1 - \frac{4}{7}\nu\right)}{\left(1 + \frac{5}{7}\nu\right)} (k_{d,0}a)^2, \tag{47}$$

where ν is the Poisson's ratio. From Eqs. (45)–(47), it is clear that in the limits of $\overline{\kappa}$, $\overline{\mu}$, and $\overline{\rho}$ approaching infinity, $\Upsilon_n \to 0$ for all the modes of interest.

In a similar manner to Eq. (1), the scattered pressure for an uncloaked rigid, immovable sphere of radius a can be written as[28]

$$p_{sc} = p_0 e^{-i\omega t} \sum_{n=0}^{\infty} i^n (2n+1)\, A_n^{(R)} h_n^{(1)}(k_{d,0}r) P_n(\cos\theta), \tag{48}$$

where p_0 is the amplitude of the incident pressure and

$$A_n^{(R)} = \frac{j_n'(k_{d,0}a)}{h_n'^{(1)}(k_{d,0}a)}. \tag{49}$$

1. Region 1: $\overline{\rho}_{c1} \gg \overline{\rho}_{c2}$

To analyze the design of a bilaminate plasmonic-type acoustic cloak for a rigid, immovable sphere, we will first

consider the analytic expressions developed in Sec. III A for the case when $\overline{\rho}_{c1} \gg \overline{\rho}_{c2}$. Taking $\Upsilon_n \to 0$, Eq. (30) for $\overline{\kappa}_{c1}$ becomes

$$\overline{\kappa}_{c1} = \frac{\delta_1 (k_{d,0} b_1)^2 [\overline{\rho}_{c1} \delta_1 k_{d,0} b_1 j_0'(k_{d,0} b_1) - \overline{\mathcal{F}}_0]}{\overline{\gamma}_0 - (k_{d,0} b_1)^2 [\overline{\rho}_{c1} \delta_1 k_{d,0} b_1 j_0'(k_{d,0} b_1) - \overline{\mathcal{F}}_0] \frac{\delta_2}{\overline{\kappa}_{c2}}}. \quad (50)$$

By examining the coefficients given by Eqs. (B1)–(B9) in the limit of $\Upsilon_n \to 0$, it is observed that $a_1^{(n)} = b_1^{(n)} = a_2^{(n)} = 0$. Therefore, Eq. (33) reduces to

$$\overline{\rho}_{c2} = 2\delta_2 \frac{a_0^{(1)} (\overline{\rho}_{c1} \delta_1)^2 + b_0^{(1)} \overline{\rho}_{c1} \delta_1 + c_0^{(1)}}{b_2^{(1)} \overline{\rho}_{c1} \delta_1 + c_2^{(1)}}. \quad (51)$$

Maintaining the restriction $(\overline{\rho}_{c1} \delta_1)^2 \ll 1$, Eq. (36) represents the solution for $\overline{\rho}_{c1}$. The sign of the square root is then selected to ensure a positive density, which corresponds to the root obtained using the "plus" sign in Eq. (36).

The expressions for q_0, q_1, and q_2 given by Eqs. (B13)–(B15) simplify considerably, no longer depending on $\overline{\kappa}_{c2}$, implying that the required values of $\overline{\rho}_{c1}$ and $\overline{\rho}_{c2}$ are independent of the bulk moduli of the cloaking layers. Furthermore, the expressions for the cloaking layer densities in Eqs. (36) and (51) show that the shell thickness δ_2 appears in the *numerator* of $\overline{\rho}_{c2}$, while the shell thickness δ_1 appears in the *denominator* of $\overline{\rho}_{c1}$. Since it has been assumed that the shell thicknesses are small, these relations dictate that cloaking of a rigid, immovable sphere occurs when $\overline{\rho}_{c1}$ is much larger than $\overline{\rho}_{c2}$.

Figures 2(a) and 2(b) illustrate the variation of $\overline{\rho}_{c1}$ with δ_1 and $\overline{\rho}_{c2}$ with δ_2, respectively. In these figures, the approximate analytic results obtained using Eqs. (36) and (51) are shown with a dashed line, and the exact numerical solution is represented by the solid line and black stars. The numerical solutions were obtained by the minimization of the scattered fields associated with the first three modes, obtained using the thin-shell results as initial guesses for each value of $\overline{\kappa}_{c2}$, denoted by the black circles. Very good agreement is observed between the approximate analytic results and the exact numerical solutions. Both highlight the dominant effects of $\overline{\rho}_{c2}$ increasing linearly with δ_2, and of $\overline{\rho}_{c1}$ varying as δ_1^{-1}. Even though the thin-shell results predict the correct functional dependence with respect to δ_1, the deviation from the exact solution increases for larger δ_1. This is due to the fact that as the shell thickness becomes thicker, the thin-shell assumptions are less accurate, as expected.

Equation (50) allows the determination of $\overline{\kappa}_{c1}$, based on the shell thickness δ_1 and the value of $\overline{\rho}_{c1}$ and $\overline{\kappa}_{c2}$. Although $\overline{\rho}_{c1}$ varies significantly with δ_1, it appears only as the product $\overline{\rho}_{c1}\delta_1$ in Eq. (50). As a function of the shell thickness, $\overline{\kappa}_{c2}$ is primarily dependent on the presence of δ_1 in the numerator, as illustrated in Fig. 3(a).

Although the shell thickness affects the magnitude of $\overline{\kappa}_{c1}$ required for cloaking, the most significant variable influencing $\overline{\kappa}_{c1}$ is $\overline{\kappa}_{c2}$. The presence of the difference between a term containing $\overline{\kappa}_{c2}$ and the coefficient $\overline{\gamma}_0$ in the denominator of Eq. (50) suggests the possibility of a pole occurring in the

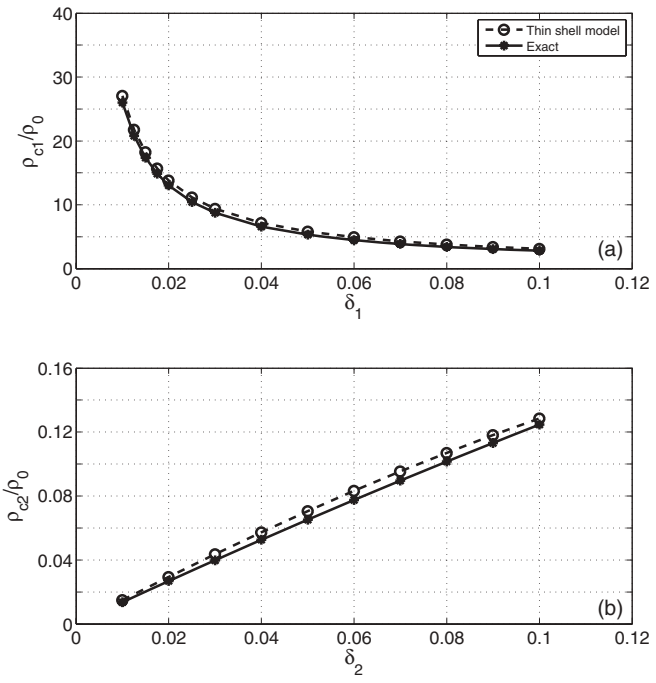

FIG. 2. Variation of cloaking layer density as a function of the shell thickness for the (a) outer cloaking layer and (b) inner cloaking layer. The two-layer-fluid cloak is enclosing a rigid, immovable sphere at $k_{d,0}a = 1.0$, with (a) $\delta_2 = 0.01$, (b) $\delta_1 = 0.01$. The cloaking layer densities are normalized by the density of the fluid in the surrounding medium, and the shell thickness is normalized by the radius of the inner sphere. Thin-shell results are calculated using Eqs. (36) and (51).

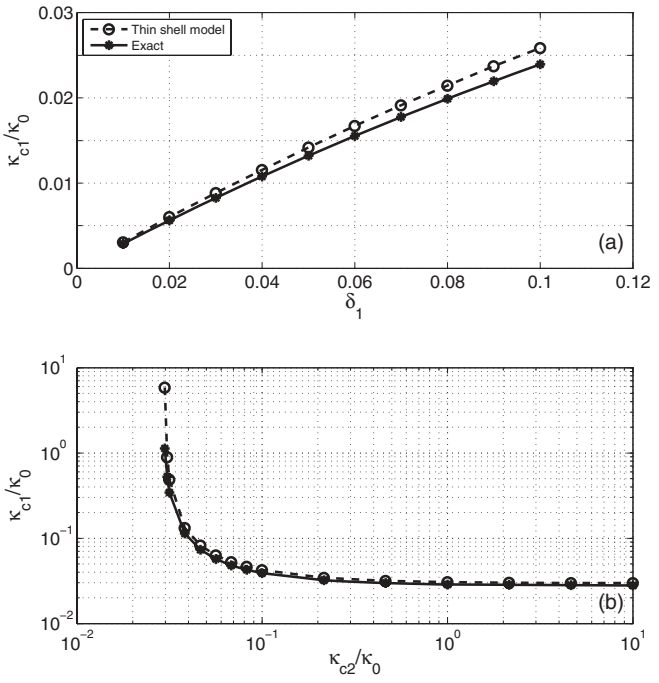

FIG. 3. Variation of the bulk modulus of the outer cloaking layer κ_{c1} as a function of the (a) shell thickness δ_1 and (b) inner cloaking layer bulk modulus κ_{c2}, enclosing a rigid, immovable sphere at $k_{d,0}a = 1.0$. In (a) $\delta_2 = 0.01$ with $\overline{\kappa}_{c1} = 1$, and in (b) $\delta_1 = \delta_2 = 0.01$. The cloaking layer bulk modulus is normalized by the bulk modulus of the fluid in the surrounding medium, and the shell thickness is normalized by the radius of the inner sphere. Thin-shell results are calculated using Eq. (50).

parameter space. This trend is observed in Fig. 3(b) in both the analytic results and exact numerical solution. For values of $\overline{\kappa}_{c2}$ below a critical point, the resulting $\overline{\kappa}_{c1}$ becomes negative. Since only positive layer properties are considered in this work, this asymptote corresponds to the minimum allowable $\overline{\kappa}_{c2}$ and sets a lower bound on the range of the parameter space. Due to the rapid rate of change as $\overline{\kappa}_{c2}$ approaches this minimum value, it can be seen that the differences in the required value of $\overline{\kappa}_{c1}$ given by the analytic model and exact solutions can become more significant. However, the analytic solution for $\overline{\kappa}_{c1}$ is still sufficient to converge to an exact solution, while capturing the underlying nature of the relationship between $\overline{\kappa}_{c1}$ and $\overline{\kappa}_{c2}$.

2. *Region 2:* $\overline{\rho}_{c1} \ll \overline{\rho}_{c2}$

In Sec. III B, analytic expressions were developed for the case when $\overline{\rho}_{c1} \ll \overline{\rho}_{c2}$. These expressions are simplified in the case of a rigid, immovable sphere, by taking the limit $\Upsilon_n \to 0$ in Eq. (38), which yields

$$\overline{\kappa}_{c2} = \frac{\delta_2 (k_{d,0} b_1)^2 [\overline{\rho}_{c2} \delta_2 k_{d,0} b_1 j_0'(k_{d,0} b_1) - \overline{\mathcal{F}}_0]}{\overline{\gamma}_0 - (k_{d,0} b_1)^2 [\overline{\rho}_{c1} \delta_1 k_{d,0} b_1 j_0'(k_{d,0} b_1) - \overline{\mathcal{F}}_0] \frac{\delta_1}{\overline{\kappa}_{c1}}}. \quad (52)$$

In the limit $\Upsilon_n \to 0$, Eqs. (B7)–(B9) and (39)–(42) yield $\bar{a}_0^{(n)} = \bar{a}_1^{(n)} = a_2^{(n)} = 0$. In this case, Eq. (43) reduces to

$$\overline{\rho}_{c1} = 2\delta_1 \frac{\bar{b}_0^{(1)} \overline{\rho}_{c2} \delta_2 + c_0^{(1)}}{b_2^{(1)} \overline{\rho}_{c2} \delta_2 + c_2^{(1)} + \bar{b}_1^{(1)} (k_{d,0} b_1)^2 \frac{\delta_1}{\overline{\kappa}_{c1}}}. \quad (53)$$

Although Eq. (43) is very similar in form to Eq. (33), an important difference is noticed in that Eq. (43) retains a dependence on $\overline{\kappa}_{c1}$, which is present in both $\bar{q}_1$ and $\bar{q}_2$ arising from $b_1^{(n)} \neq 0$. The dependence of $\overline{\kappa}_{c2}$, $\overline{\rho}_{c2}$, and $\overline{\rho}_{c1}$ on $\overline{\kappa}_{c1}$ is shown Figs. 4(a)–4(c), respectively.

From Figs. 4(a) and 4(b), both $\overline{\kappa}_{c2}$ and $\overline{\rho}_{c2}$ asymptotically become infinite as $\overline{\kappa}_{c1}$ decreases towards a critical point, beyond which the required cloaking layer properties are negative. This asymptotic behavior is also observed in the required value of $\overline{\rho}_{c1}$ in Fig. 4(c), except that it asymptotes to $-\infty$.

Another important characteristic for this case is the presence of a lower limit for the positive values of $\overline{\rho}_{c2}$ and $\overline{\kappa}_{c2}$, which occur as $\overline{\kappa}_{c1} \to \infty$. For $\overline{\rho}_{c2}$, this leads to values which are quite large; for $\delta_1 = 0.01$ illustrated in Fig. 4, the lower limit is $\overline{\rho}_{c2} = 1879$. Aside from the practical problems of achieving such a high density for certain surrounding fluids, this leads to $k_{d,c2} b_1 \delta_2 \approx 1$, which suggests that the layer is not small enough compared to the wavelength to be considered thin, and would require retaining higher-order terms to achieve sufficient accuracy.

B. Effects of elasticity

In this section, the effects of elasticity in the core and in the cloaking layers will be investigated. First, the case of a penetrable isotropic elastic sphere will be considered. After exploring the behavior of various common elastic solids, the details of the resulting reduction in the scattering strength will be examined for a specific case of a steel sphere in water. Using this example, the broad applicability of the equations developed in Sec. III A will be illustrated for both a two-fluid cloaking layer configuration and when elastic (shear) effects are considered in the outer cloaking layer.

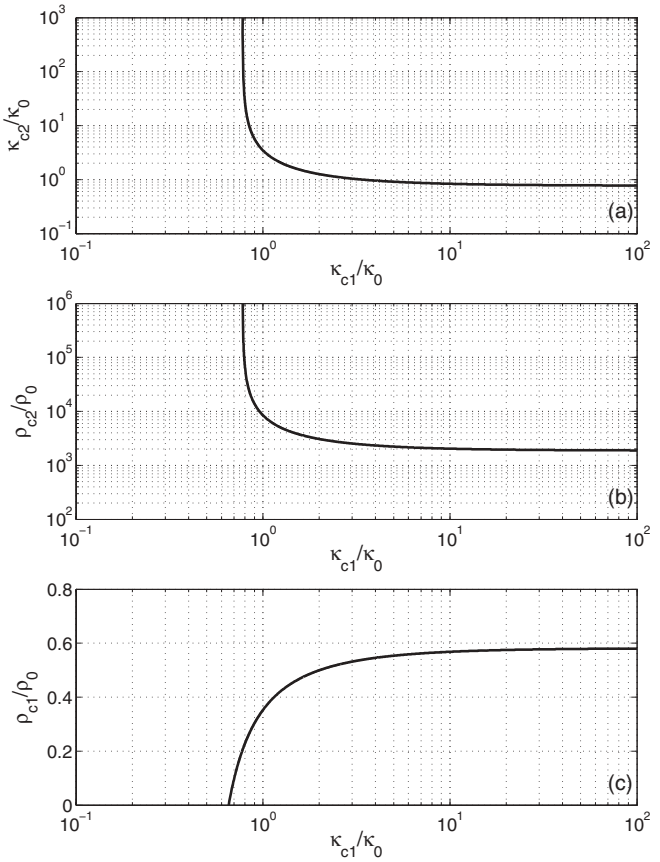

FIG. 4. Variation as a function of outer cloaking layer bulk modulus κ_{c1} for (a) the inner cloaking layer bulk modulus κ_{c2}, (b) the outer cloaking layer density ρ_{c2}, and (c) the inner cloaking layer density ρ_{c1}, enclosing a rigid, immovable sphere for $\delta_1 = \delta_2 = 0.01$ at $k_{d,0}a = 2.0$. The cloaking layer properties are normalized by those of the fluid in the surrounding medium. Thin-shell results are calculated using Eqs. (44), (52), and (53).

1. *Cloaking of a penetrable elastic core*

To examine the cloaking layer properties when the core material is an isotropic elastic solid, Fig. 5 shows $\overline{\rho}_{c1}$, $\overline{\rho}_{c2}$, and $\overline{\kappa}_{c1}$ as a function of $\overline{\kappa}_{c2}$ for $\delta_1 = \delta_2 = 0.04$ and $k_{d,0}a = 2.0$. The results for three different isotropic elastic solids commonly used in engineering applications are presented: steel, aluminum, and glass. The surrounding fluid in each case is water. For comparison, the results for a rigid, immovable sphere are also shown.

Comparing the results for the three elastic solids to that of the rigid sphere, the same general trends can be found for each cloaking layer property. In Fig. 5(a), $\overline{\kappa}_{c1}$ exhibits the same asymptotic behavior for all cases, although the point where $\overline{\kappa}_{c1} \to \infty$ occurs at a slightly lower value of $\overline{\kappa}_{c2}$ for the elastic core materials.

In Fig. 5(b), the variation in $\overline{\rho}_{c1}$ with $\overline{\kappa}_{c2}$ is illustrated. It can be observed that elastic core materials exhibit a slight decrease in the relative value of $\overline{\rho}_{c1}$ for smaller values of $\overline{\kappa}_{c2}$. This is in contrast with the case of a rigid, immovable core, which was seen in the previous section to be independent of $\overline{\kappa}_{c2}$.

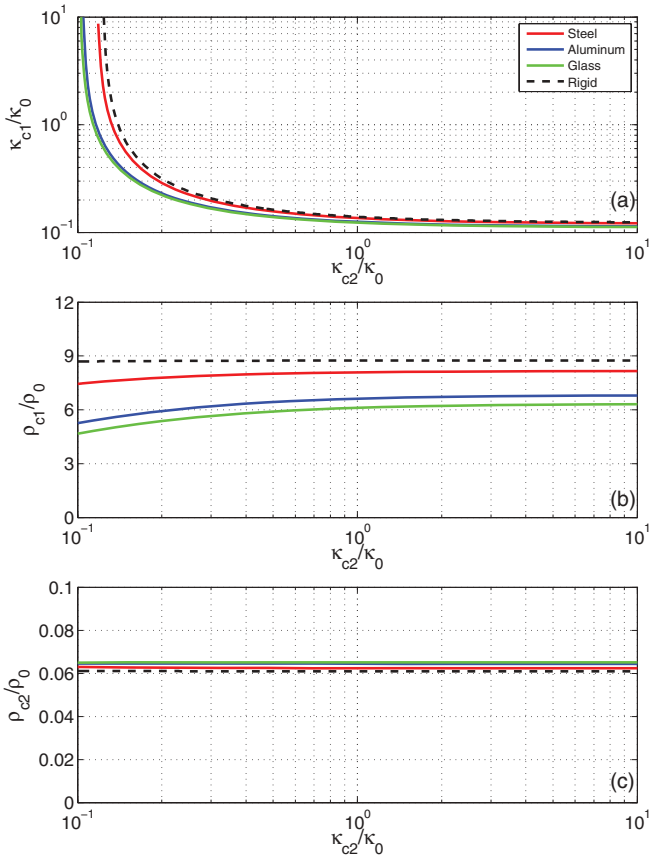

FIG. 5. (Color online) Variation as a function of inner cloaking layer bulk modulus κ_{c2} of (a) the outer cloaking layer bulk modulus κ_{c1}, (b) the inner cloaking layer density ρ_{c1}, and (c) the outer cloaking layer density ρ_{c2} for $\delta_1 = \delta_2 = 0.04$ at $k_{d,0}a = 2.0$. Curves are shown for four different core materials: steel (solid red line), aluminum (solid blue line), glass (solid green line), and a rigid, immovable sphere (dashed black line). Material properties are obtained from Kinsler *et al.*[29] The cloaking layer properties are normalized by those of the fluid in the surrounding medium, which is water. Thin-shell results are calculated using Eqs. (36), (50), and (51).

However, the most significant variation occurs in the overall magnitude of $\overline{\rho}_{c1}$, which decreases with the density and bulk modulus of the elastic material. Specifically, it can be observed that the value of $\overline{\rho}_{c1}$ required in this configuration for a glass or aluminum sphere is about one-third that of a rigid sphere. Even for a steel sphere, with a density and bulk modulus much larger than water, the cloak properties are still about 10% less than if the sphere were perfectly rigid.

Figure 5(c) illustrates the variation of $\overline{\rho}_{c2}$, which shows that this parameter is much less sensitive to the core material properties, compared to $\overline{\rho}_{c1}$. The small change in the magnitude which arises when considering elastic core materials leads to slightly larger value of $\overline{\rho}_{c2}$. In addition, there is negligible change as $\overline{\kappa}_{c2}$ is varied over several orders of magnitude.

In the analysis of the bilaminate plasmonic-type acoustic cloak up to this point, the focus has been on determining the necessary cloaking layer properties and understanding their relationship to achieve an optimal design. To explore the functionality of the cloak, consider now a steel sphere in water, covered by two fluid cloaking layers with thicknesses $\delta_1 = \delta_2 = 0.04$, $\overline{\kappa}_{c2} = 0.175$ and a design frequency of $k_{d,0}a = 2.0$. The cloaking layer properties used for this case are given in Table I.

TABLE I. Cloaking layer properties for a bilaminate plasmonic-type acoustic cloak for a steel sphere in water, consisting of two layers with shell thicknesses $\delta_1 = \delta_2 = 0.04$ and a design frequency of $k_{d,0}a = 2.0$. Solutions are given based on analytic thin-shell expressions, exact solutions for the case of two fluid layers, and exact solutions for the case of a fluid inner layer and isotropic elastic outer layer with $\nu_{c1} = 0.3$.

Solution type	$\overline{\rho}_{c1}$	$\overline{\kappa}_{c1}$	$\overline{\rho}_{c2}$	$\overline{\kappa}_{c2}$
Analytic (thin-shell approx.)	7.738	0.361	0.063	0.175
Exact (fluid/fluid)	7.700	0.213	0.049	0.175
Exact (elastic/fluid)	8.081	0.262	0.056	0.175

To examine the effectiveness of the cloak at $k_{d,0}a = 2.0$, Figs. 6(a) and 6(b) show the real part of the total pressure field for an uncloaked and cloaked steel sphere in water subjected to a time-harmonic incident pressure wave traveling from bottom to top. For the uncloaked sphere shown in Fig. 6(a), there is significant perturbation of the pressure field around the object and of the stress field within the sphere.

Figure 6(b) indicates that the optimized cloaking layers dramatically change the pressure field in the surrounding fluid and within the elastic sphere, showing that the incident wave is almost completely undisturbed by the cloaked sphere. Since the plasmonic-type acoustic cloak was designed to cancel the scattered field in the surrounding fluid, it is also seen that the incident pressure field still interacts with the steel sphere, resulting in a stress field within the sphere which is much more uniform than when uncloaked. With the scattered field canceled, the total pressure acting on the outer surface of the steel sphere is equal to the incident pressure, and so the stresses in the steel sphere are phase matched to the incoming wave. One interesting take-away from this observation is that this type of cloak therefore enables the design of an *ideal sensor*, allowing for detection on an incident acoustic wave without almost any disruption of the pressure field.[30,31]

To analyze the frequency dependence of the plasmonic-type acoustic cloak functionality, the magnitude of the first six scattering coefficients is plotted for the uncloaked and cloaked

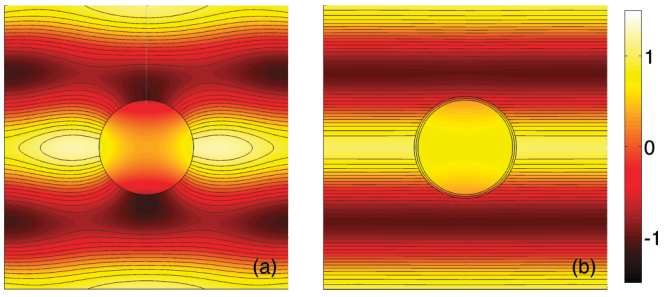

FIG. 6. (Color online) Real part of the total pressure field for a steel sphere in water at $k_{d,0}a = 2.0$: (a) uncloaked, (b) cloaked using two fluid layers. For the cloaked sphere, each layer of the cloak has a shell thickness of $\delta = 0.04$. The color scale for the pressure is normalized by the amplitude for the incident wave, which is a time-harmonic plane wave traveling from bottom to top.

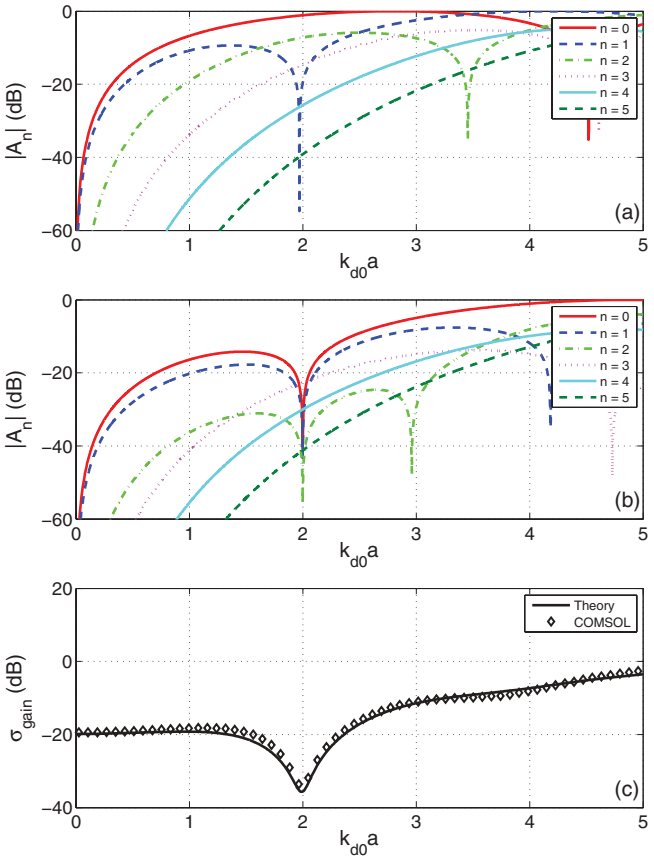

FIG. 7. (Color online) Scattering coefficients (in dB) for an (a) uncloaked and (b) cloaked steel sphere in water. The cloak consists of two fluid layers with $\delta_1 = \delta_2 = 0.04$, which cancels the first three scattering modes at $k_{d,0}a = 2.0$. The scattering gain in dB, relative to the uncloaked scatterer, is given in (c) for the exact theoretical solution and using finite elements (COMSOL).

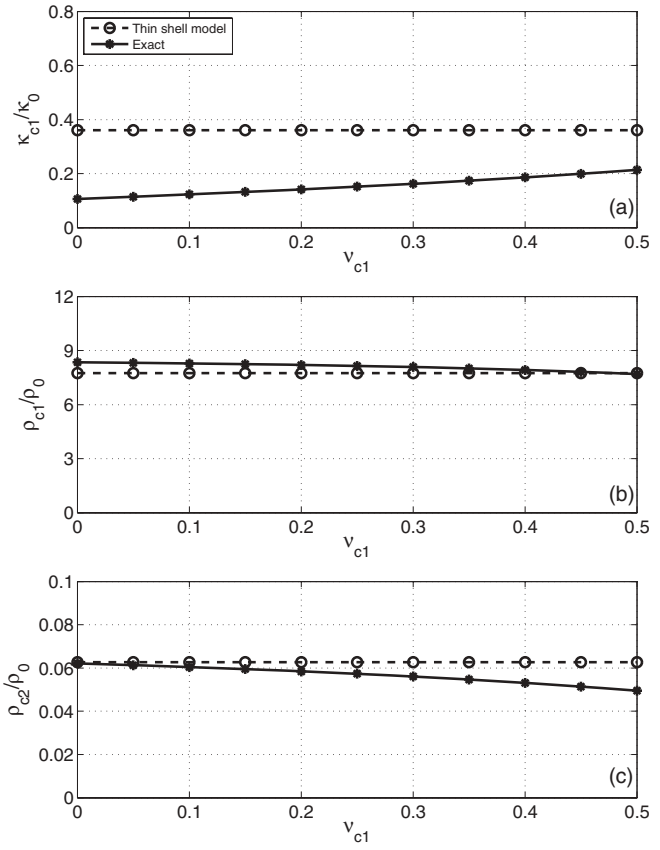

FIG. 8. Variation as a function of the outer cloaking layer Poisson's ratio ν_{c1} for (a) the outer cloaking layer bulk modulus κ_{c1}, (b) the inner cloaking layer density ρ_{c1}, and (c) the outer cloaking layer density ρ_{c2}, enclosing a steel sphere in water for $\delta_1 = \delta_2 = 0.04$ at $k_{d,0}a = 2.0$. The cloaking layer properties are normalized by those of the fluid in the surrounding medium. Thin-shell results are calculated using Eqs. (36), (50), and (51).

configurations in Figs. 7(a) and 7(b), respectively. In Fig. 7 (a), it is noted that each mode has modal nulls at some frequencies, even in the absence of cloaking layers. The effect of adding the cloaking layer is clearly seen by comparing Figs. 7(a) and 7(b) at the design frequency of $k_{d,0}a = 2.0$, where nulls in the $n = 0$, 1, and 2 scattering modes are aligned. From these plots, it is observed that the role of the cloak is to line up all the nulls for the relevant scattering orders.

The resulting scattered field at the design frequency can be expressed in terms of the scattering gain, which is plotted in Fig. 7(c). From this plot, it can be seen that the scattering strength is reduced by 35 dB at $k_{d,0}a = 2.0$, where the first three scattering modes are canceled. Interestingly, away from the design frequency, significant scattering reduction is also obtained. In particular, the scattering strength is reduced by 20 dB over a range of $k_{d,0}a$ from 0 to almost 2.5. This reduction in scattering strength, although more modest, extends up to $k_{d,0}a = 5$ and beyond.

To verify the methods and results developed throughout this work, the COMSOL multiphysics software package was utilized. Unlike the spherical harmonic expansions used here, COMSOL uses finite-element analysis to solve problems of arbitrary two- (2D) and three-dimensional (3D) geometries. A 2D axisymmetric model was developed using the acoustics module in COMSOL to simulate the geometry given by Fig. 1 for the cloak properties tabulated in Table I. A comparison of the scattering gain calculated using the analytic expressions developed in Sec. III and COMSOL presented in Fig. 7(c). From this plot, excellent agreement is observed over the entire band shown.

2. *Practical considerations for implementation*

Given the ability of the plasmonic-type acoustic cloak described in the previous section to significantly reduce the scattering strength of a spherical target in water, an important question to consider is what type of materials could be used to create such a structure. The cloaking layer properties presented in the previous section require two fluid layers, with the cloaking layer properties given in Table I. For the specific case considered here, the bulk modulus of each layer is approximately 0.2 times that of water. The density of the outer layer needs to be large, roughly equal to that of steel, while the density of the inner layer is very low, about 5% of the density of water.

Since no naturally occurring fluids exhibit such properties, alternative methods would be required to obtain the necessary combinations of densities and bulk moduli. One possible means would be the use of acoustic metameri-

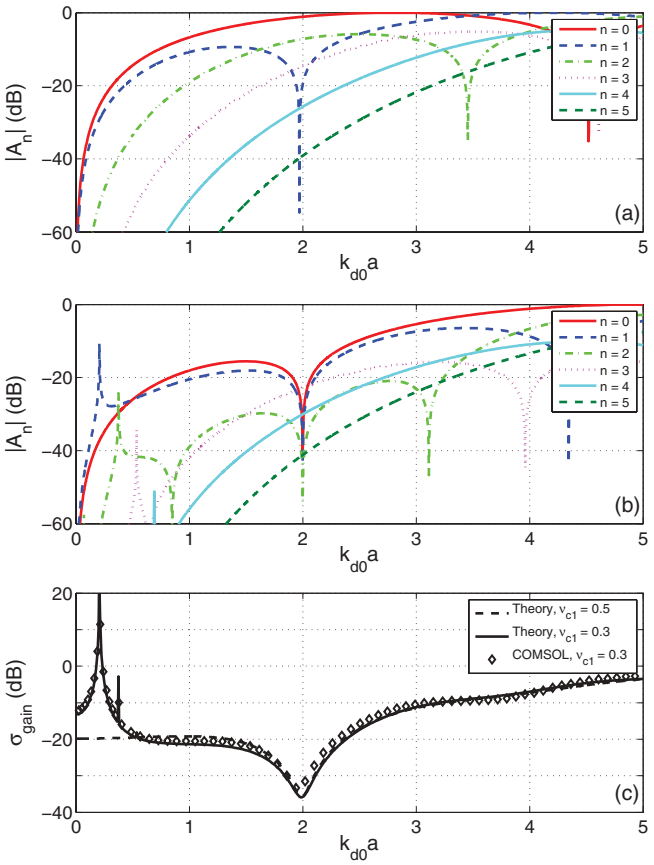

FIG. 9. (Color online) Scattering coefficients (in dB) for an (a) uncloaked and (b) cloaked steel sphere in water. The cloak consists of an inner fluid layer and outer elastic layer with $\delta_1 = \delta_2 = 0.04$, which cancels the first three scattering modes at $k_{d,0}a = 2.0$. The Poisson's ratio of the outer elastic layer is 0.3. The scattering gain in dB, relative to the uncloaked scatterer, is given in (c) for the exact theoretical solution and using finite elements (COMSOL) for the case when the outer layer is an isotropic elastic solid. The scattering gain for the case of a fluid outer layer (dashed) is given for reference.

als, which have been proposed for other acoustic cloaking applications.[6,16,26,32,33] Unlike acoustic cloaks developed using coordinate transformation techniques, the layers for this design are simply isotropic fluids, but require extreme values not found in nature.

One promising method to achieve the necessary material properties consists in creating an effective fluid using a microstructure consisting of smooth beads. Such a structure would allow for the density and bulk modulus of the effective fluid to be varied based on the composition and volume fraction of the beads. Use of a lubricated bead microstructure has also been proposed as a means for creating an *acoustic metafluid*, based on the requirements for a transformation-based acoustic cloak.[6]

Although the design procedure presented in this paper has assumed that the cloak consists of two fluid layers, in practice this would require some sort of elastic materials to maintain the structure of the cloak. To determine the effect of using an isotropic elastic solid for the outer layer, Fig. 8 shows the variation of the cloaking layer properties with the Poisson's ratio in the outer layer ν_{c1}. Using the thin-fluid-shell model results as an initial guess, the exact solution for each value of ν_{c1} was determined using the numerical techniques described in Sec. II. Since the analytic thin-shell expressions developed in this work assume only fluid layers, these results tacitly assume a Poisson's ratio of 0.5 in the cloaking layers and therefore appear constant in the plots. Although there is some deviation in the magnitude of the cloaking layer properties required when the outer layer is elastic compared to the fluid layer solution, the difference is relatively modest and suggests that the use of the analytic results developed in Sec. III can be applied to get a good initial guess also when the outer layer is elastic.

Figures 9(a) and 9(b) show the magnitude of the first six scattering coefficients plotted for the uncloaked and cloaked configuration with $\nu_{c1} = 0.3$, respectively, using the cloaking layer properties listed in Table I. The scattering gain is presented in Fig. 9(c), with the elastic layer and the fluid-only cloaking layer solution shown together for comparison. In the vicinity of the design frequency $k_{d,0}a = 2.0$ and above, the scattering modes and scattering gain are nearly identical to the case with two fluid layers. At low frequencies, however, there is a large peak in the the scattering gain. This is associated with the $n = 1$ (dipole) resonance within the outer cloaking layer itself, which arises from the excitation of axisymmetric Lamb waves, and its behavior is also captured with remarkable precision using COMSOL. These resonances can also be found in the higher-order modes, although the increase in the scattering gain is dominated by the response from the dipole mode.

V. CONCLUSIONS

To conclude, the behavior of a bilaminate plasmonic-type acoustic cloak has been investigated in detail throughout this work. We have derived an exact solution for the properties of a plasmonic-type acoustic cloak to cancel the scattered field from a spherical object. This solution requires implicit numerical techniques. As a result, a reasonable estimate of the cloaking layer properties are needed *a priori* to formulate an initial guess, and to ensure that the obtained solution represents a global minimum for the scattered field. Analytic expressions were developed using thin-shell assumptions, which provide explicit solutions for the cloaking layer properties. These expressions provide valuable insight into what type of properties are needed in the cloak, and the dependence of these properties on the various other design parameters. In addition, within all the considered cloaking designs, these approximate formulas match very well with the exact numerical solutions.

By examining the governing equations within the thin-shell approximation, it is shown that inertial effects of the two layers represent the dominant mechanism that ensure the cancellation of a sufficient number of scattering modes. In the examination of these inertial effects, two scenarios have been considered: (1) when the outer layer is much denser than the inner layer, and (2) the inner layer is much denser than the outer layer. Although both regions satisfy the requirements for cancellation of the scattered field, those involving the case where the outer layer is much denser provide a far more robust solution involving more feasible cloaking layer properties. For the case when the inner layer is much denser, the cloaking layer properties exhibit a strong dependence on the bulk moduli of the cloaking layers,

and ultimately lead to solutions in which the cloaking layers do not behave as thin shells.

Based on this analysis, the performance of a bilaminate plasmonic-type acoustic cloak with an outer layer much denser than the inner layer has been examined, and practical means of achieving the desired cloaking layer properties have been discussed. Using the explicit cloaking layer expressions derived in this paper, a bilaminate shell consisting of two cloaking layers has been formulated for a steel sphere in water at $k_{\mathrm{d},0}a = 2$. At the design frequency, a 35-dB reduction in the scattering strength is obtained, with a more moderate reduction in the scattering strength extending beyond $k_{\mathrm{d},0}a = 5$. A reduction of 20 dB or more below the design frequency is observed using two fluid cloaking layers, although the presence of elastic effects in the outer layer can lead to asymmetric Lamb mode (plate wave) resonances in this low-frequency region. This example demonstrates the effectiveness and potential of a bilaminate plasmonic-type acoustic cloak in broadband reduction of the scattered field, and the usefulness of the analytic expressions for the cloaking layer properties as a design tool.

APPENDIX A: COEFFICIENTS OF $\mathrm{U}^{(n)}$ MATRIX

The coefficients of the $\mathrm{U}^{(n)}$ matrix are

$$u_{11}^{(n)} = k_{\mathrm{d},0}b\, j_n'(k_{\mathrm{d},0}b), \tag{A1}$$

$$u_{12}^{(n)} = k_{\mathrm{d,c}1}b\, j_n'(k_{\mathrm{d,c}1}b), \tag{A2}$$

$$u_{13}^{(n)} = k_{\mathrm{d,c}1}b\, n_n'(k_{\mathrm{d,c}1}b), \tag{A3}$$

$$u_{21}^{(n)} = j_n(k_{\mathrm{d},0}b), \tag{A4}$$

$$u_{22}^{(n)} = \overline{\rho}_{\mathrm{c}1}\, j_n(k_{\mathrm{d,c}1}b), \tag{A5}$$

$$u_{23}^{(n)} = \overline{\rho}_{\mathrm{c}1}\, n_n(k_{\mathrm{d,c}1}b), \tag{A6}$$

$$u_{32}^{(n)} = k_{\mathrm{d,c}1}b_1\, j_n'(k_{\mathrm{d,c}1}b_1), \tag{A7}$$

$$u_{33}^{(n)} = k_{\mathrm{d,c}1}b_1\, n_n'(k_{\mathrm{d,c}1}b_1), \tag{A8}$$

$$u_{34}^{(n)} = -k_{\mathrm{d,c}2}b_1\, j_n'(k_{\mathrm{d,c}2}b_1), \tag{A9}$$

$$u_{35}^{(n)} = -k_{\mathrm{d,c}2}b_1\, n_n'(k_{\mathrm{d,c}2}b_1), \tag{A10}$$

$$u_{42}^{(n)} = \overline{\rho}_{\mathrm{c}1}\, k_{\mathrm{d,c}1}b_1\, j_n(k_{\mathrm{d,c}1}b_1), \tag{A11}$$

$$u_{43}^{(n)} = \overline{\rho}_{\mathrm{c}1}\, k_{\mathrm{d,c}1}b_1\, n_n(k_{\mathrm{d,c}1}b_1), \tag{A12}$$

$$u_{44}^{(n)} = -\overline{\rho}_{\mathrm{c}2}\, k_{\mathrm{d,c}2}b_1\, j_n(k_{\mathrm{d,c}2}b_1), \tag{A13}$$

$$u_{45}^{(n)} = -\overline{\rho}_{\mathrm{c}2}\, k_{\mathrm{d,c}2}b_1\, n_n(k_{\mathrm{d,c}2}b_1), \tag{A14}$$

$$u_{54}^{(n)} = k_{\mathrm{d,c}2}a\, j_n'(k_{\mathrm{d,c}2}a), \tag{A15}$$

$$u_{55}^{(n)} = k_{\mathrm{d,c}2}a\, n_n'(k_{\mathrm{d,c}2}a), \tag{A16}$$

$$u_{56}^{(n)} = -k_{\mathrm{d}}a\, j_n'(k_{\mathrm{d}}a), \tag{A17}$$

$$u_{57}^{(n)} = -n(n+1)\, j_n(k_{\mathrm{s}}a), \tag{A18}$$

$$u_{64}^{(n)} = \overline{\rho}_{\mathrm{c}2}\, j_n(k_{\mathrm{d,c}2}a), \tag{A19}$$

$$u_{65}^{(n)} = \overline{\rho}_{c2}\, n_n(k_{\mathrm{d,c}2}a), \tag{A20}$$

$$u_{66}^{(n)} = 2\overline{\rho}\left\{\left[\frac{n(n+1)}{(k_{\mathrm{s}}a)^2} - \frac{1}{2}\right] j_n(k_{\mathrm{d}}a) - 2\frac{k_{\mathrm{d}}a}{(k_{\mathrm{s}}a)^2}\, j_n'(k_{\mathrm{d}}a)\right\}, \tag{A21}$$

$$u_{67}^{(n)} = 2\overline{\rho}\frac{n(n+1)}{(k_{\mathrm{s}}a)^2}[k_{\mathrm{s}}a j_n'(k_{\mathrm{s}}a) - j_n(k_{\mathrm{s}}a)], \tag{A22}$$

$$u_{76}^{(n)} = k_{\mathrm{d}}a\, j_n'(k_{\mathrm{d}}a) - j_n(k_{\mathrm{d}}a), \tag{A23}$$

$$u_{77}^{(n)} = \left[n(n+1) - 1 - \frac{1}{2}(k_{\mathrm{s}}a)^2\right] j_n(k_{\mathrm{s}}a) - k_{\mathrm{s}}a\, j_n'(k_{\mathrm{s}}a), \tag{A24}$$

with $\overline{\rho}_{\mathrm{c}1} = \rho_{\mathrm{c}1}/\rho_0$, $\overline{\rho}_{\mathrm{c}2} = \rho_{\mathrm{c}2}/\rho_0$, and $\overline{\rho} = \rho/\rho_0$.

APPENDIX B: COEFFICIENTS FOR WHEN $\overline{\rho}_{\mathrm{c}1} \gg \overline{\rho}_{\mathrm{c}2}$

The coefficients for Eq. (32) are

$$a_0^{(n)} = -k_{\mathrm{d},0}b_1\, j_n'(k_{\mathrm{d},0}b_1)\overline{\mathcal{G}}_0, \tag{B1}$$

$$b_0^{(n)} = \overline{\mathcal{F}}_n\overline{\mathcal{G}}_0 + k_{\mathrm{d},0}b_1\, j_n'(k_{\mathrm{d},0}b_1)\overline{\mathcal{F}}_0, \tag{B2}$$

$$c_0^{(n)} = -\overline{\mathcal{F}}_0\overline{\mathcal{F}}_n, \tag{B3}$$

$$a_1^{(n)} = k_{\mathrm{d},0}b_1[\Upsilon_0 j_0(k_{\mathrm{d},0}b_1) j_n'(k_{\mathrm{d},0}b_1) - \Upsilon_n j_n(k_{\mathrm{d},0}b_1) j_0'(k_{\mathrm{d},0}b_1)], \tag{B4}$$

$$b_1^{(n)} = -[\Upsilon_0 j_0(k_{\mathrm{d},0}b_1)\overline{\mathcal{F}}_n - \Upsilon_n j_n(k_{\mathrm{d},0}b_1)\overline{\mathcal{F}}_0], \tag{B5}$$

$$c_1^{(n)} = 0, \tag{B6}$$

$$a_2^{(n)} = \Upsilon_n\overline{\mathcal{F}}_n\overline{\mathcal{G}}_0 - \Upsilon_0\overline{\mathcal{F}}_0\overline{\mathcal{G}}_n, \tag{B7}$$

$$b_2^{(n)} = [\overline{\gamma}_n\overline{\mathcal{G}}_0 - \overline{\gamma}_0\overline{\mathcal{G}}_n] - [\Upsilon_n\overline{\mathcal{F}}_n\overline{\mathcal{G}}_0 - \Upsilon_0\overline{\mathcal{F}}_0\overline{\mathcal{G}}_n], \tag{B8}$$

$$c_2^{(n)} = -[\overline{\gamma}_n\overline{\mathcal{F}}_0 - \overline{\gamma}_0\overline{\mathcal{F}}_n], \tag{B9}$$

$$a_3^{(n)} = 0, \tag{B10}$$

$$b_3^{(n)} = \Upsilon_n j_n(k_{\mathrm{d},0}b_1)\overline{\mathcal{G}}_0 - \Upsilon_0 j_0(k_{\mathrm{d},0}b_1)\overline{\mathcal{G}}_n, \tag{B11}$$

$$c_3^{(n)} = -[\Upsilon_n j_n(k_{\mathrm{d},0}b_1)\overline{\mathcal{F}}_0 - \Upsilon_0 j_0(k_{\mathrm{d},0}b_1)\overline{\mathcal{F}}_n]. \tag{B12}$$

Using Eqs. (B1)–(B9), the coefficients in Eq. (35) can be defined as

$$q_0 = 2c_0^{(1)}c_2^{(2)} - 6c_0^{(2)}c_2^{(1)}, \tag{B13}$$

$$q_1 = 2\left[b_0^{(1)}c_2^{(2)} + c_0^{(1)}\left(b_2^{(2)} + b_1^{(2)}\overline{\chi}_{\mathrm{c}2}\right)\right] - 6\left[b_0^{(2)}c_2^{(1)} + c_0^{(2)}\left(b_2^{(1)} + b_1^{(1)}\overline{\chi}_{\mathrm{c}2}\right)\right], \tag{B14}$$

$$q_2 = 2\left[a_0^{(1)}c_2^{(2)} + b_0^{(1)}\left(b_2^{(2)} + b_1^{(2)}\overline{\chi}_{\mathrm{c}2}\right) + c_0^{(1)}\left(a_2^{(2)} + a_1^{(2)}\overline{\chi}_{\mathrm{c}2}\right)\right] - 6\left[a_0^{(2)}c_2^{(1)} + b_0^{(2)}\left(b_2^{(1)} + b_1^{(1)}\overline{\chi}_{\mathrm{c}2}\right) + c_0^{(2)}\left(a_2^{(1)} + a_1^{(1)}\overline{\chi}_{\mathrm{c}2}\right)\right]. \tag{B15}$$

*mdguild@utexas.edu

[1]A. Alù and N. Engheta, Phys. Rev. E **72**, 016623 (2005).
[2]D. Rainwater, A. Kerkhoff, K. Melin, J. C. Soric, G. Moreno, and A. Alù, New J. Phys. **14**, 013054 (2012).
[3]M. D. Guild, A. Alù, and M. R. Haberman, J. Acoust. Soc. Am. **129**, 1355 (2011).
[4]M. D. Guild, M. R. Haberman, and A. Alù, Wave Motion **48**, 468 (2011).
[5]U. Leonhardt, Science **312**, 1777 (2006).
[6]A. N. Norris, Proc. R. Soc. A **464**, 2411 (2008).
[7]A. Alù and N. Engheta, Phys. Rev. Lett. **102**, 233901 (2009).
[8]A. Alù and N. Engheta, Phys. Rev. Lett. **105**, 263906 (2010).
[9]A. Greenleaf, Y. Kurylev, M. Lassas, U. Leonhardt, and G. Uhlmann, Proc. Natl. Acad. Sci. USA **109**, 10169 (2012).
[10]H. Shen, M. P. Païdoussis, J. Wen, D. Yu, L. Cai, and X. Wen, J. Phys. D: Appl. Phys. **45**, 285401 (2012).
[11]X. Zhu, B. Liang, W. Kan, X. Zou, and J. Cheng, Phys. Rev. Lett. **106**, 014301 (2011).
[12]T. Xu, X.-F. Zhu, B. Liang, Y. Li, X.-Y. Zou, and J.-C. Cheng, Appl. Phys. Lett. **101**, 033509 (2012).
[13]N. A. Nicorovici, G. W. Milton, R. C. McPhedran, and L. C. Botten, Opt. Express **15**, 6314 (2007).
[14]A. Alù and N. Engheta, Phys. Rev. Lett. **100**, 113901 (2008).
[15]M. Schoenberg and P. N. Sen, J. Acoust. Soc. Am. **73**, 61 (1983).
[16]D. Torrent and J. Sánchez-Dehesa, New. J. Phys.**10**, 063015 (2008).
[17]Y. Cheng, F. Yang, J. Y. Xu, and X. J. Liu, Appl. Phys. Lett. **92**, 151913 (2008).
[18]J. J. Faran, J. Acoust. Soc. Am. **23**, 405 (1951).
[19]R. R. Goodman and R. Stern, J. Acoust. Soc. Am. **34**, 338 (1962).
[20]R. Hickling, J. Acoust. Soc. Am. **34**, 1582 (1962).
[21]R. Hickling, J. Acoust. Soc. Am. **34**, 1124 (1964).
[22]G. C. Gaunaurd, Appl. Mech. Rev. **42**, 143 (1989).
[23]L. W. Anson and R. C. Chivers, J. Acoust. Soc. Am. **93**, 1687 (1993).
[24]MATLAB, *Optimization Toolbox*, version 7.8.0 (R2009a) (The MathWorks, Inc., Natick, Massachusetts, 2009).
[25]M. Abramowitz and I. A. Stegun, *Handbook of Mathematical Functions: With Formulas, Graphs and Mathematical Tables* (Dover, New York, 1972).
[26]S. A. Cummer and D. Schurig, New J. Phys. **9**, 45 (2007).
[27]L. Landau, E. Lifshitz, A. Kosevich, and L. Pitaevskiĭ, *Theory of Elasticity*, Theoretical Physics (Butterworth-Heinemann, Oxford, UK, 1986).
[28]M. C. Junger and D. Feit, *Sound, Structures, and Their Interaction* (The Acoustical Society of America, New York, 1993).
[29]L. E. Kinsler, A. R. Frey, A. B. Coppens, and J. V. Sanders, *Fundamentals of Acoustics*, 4th ed. (Wiley, New York, 2000).
[30]A. Alù and N. Engheta, Metamaterials **4**, 153 (2010).
[31]M. D. Guild, M. R. Haberman, and A. Alù, J. Acoust. Soc. Am. **129**, 2643 (2011).
[32]D. Torrent and J. Sánchez-Dehesa, New. J. Phys. **10**, 023004 (2008).
[33]S. Zhang, C. Xia, and N. Fang, Phys. Rev. Lett. **106**, 024301 (2011).